Inorganic Chemistry

Article

pubs.acs.org/IC

Structure, Phase Transition Behaviors and Electrical Properties of Nd Substituted Aurivillius Polycrystallines $Na_{0.5}Nd_xBi_{2.5-x}Nb_2O_9$ (x = 0.1, 0.2, 0.3, and 0.5)

Changbai Long, Huiqing Fan,* and Pengrong Ren

State Key Laboratory of Solidification Processing, School of Materials Science and Engineering, Northwestern Polytechnical University, Xi'an 710072, P. R. China

Supporting Information

ABSTRACT: New high temperature Aurivillius piezoelectrics $Na_{0.5}Nd_xBi_{2.5-x}Nb_2O_9$ (NDBNx, x = 0.1, 0.2, 0.3, and 0.5) with Nd substitution for Bi at the A site were synthesized using a solid state reaction process. Crystal structures of NDBN0.2 and NDBN0.5 were refined with the Rietveld method with powder X-ray diffraction, and they crystallized in the orthorhombic space group $A2_1am$ [a = 5.48558(8) Å, b = 5.46326(9) Å, c = 24.8940(4) Å, and Z = 4 for NDBN0.2 and a = 5.46872(5) Å, b = 5.46730(5) Å, c = 24.80723(25) Å, and Z = 4 for NDBN0.5], at room temperature. The refinement results and Raman spectroscopy of NDBNx verified that Nd occupied both the A site in the perovskite layers and the cation site in the $(Bi_2O_2)^{2+}$ layers. The Nd substitution induced an enhancement in cation disordering between the A site and the $(Bi_2O_2)^{2+}$ layer and an increase in the degree of the relaxation behavior for NDBNx. The ferroelectric to paraelectric phase transition temperature (T_c) of NDBNx ranged from 735 to 764 °C. Furthermore, the isovalent substitution of Nd for Bi had a great influence on microstructure (grain size and shape), defect concentration (mainly oxygen vacancies), preferred grain orientation (texture), and distortion of the octahedron. The coaction between these effects determined the structure characteristics, phase transition behaviors, and electrical properties of NDBNx.

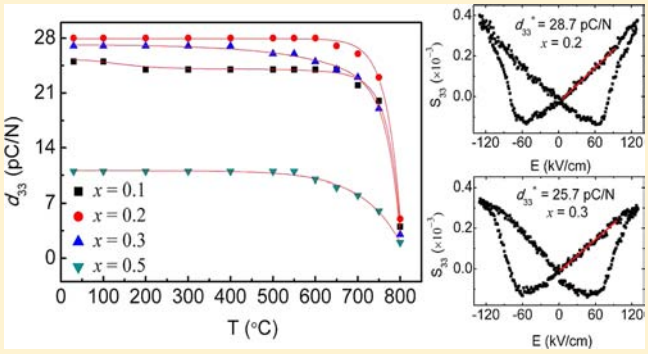

1. INTRODUCTION

Aurivillius ferroelectrics (bismuth layer structure ferroelectrics, BLSFs) are thought to be promising candidates for nonvolatile ferroelectric random access memories (NvFRAMs) and high temperature piezoelectric transducers, compared with Pb-$(Zr,Ti)O_3$ (PZT) and other lead-free materials.[1−9] Aurivillius ferroelectrics possess excellent fatigue-resistant properties, e.g., $SrBi_2Ta_2O_9$ (SBT) and $Bi_{3.25}La_{0.75}Ti_3O_{12}$ (BLT).[1,2] They also have high Curie point (T_c) and high temperature stability, e.g., Bi_3TiNbO_9 (BTN) and $CaBi_2Nb_2O_9$ (CBN).[4,5,10] The general formula of BLSFs is $(Bi_2O_2)^{2+}(A_{n-1}B_nO_{3n+1})^{2-}$, where A is Ca^{2+}, Sr^{2+}, Ba^{2+}, Pb^{2+}, Bi^{3+}, K^+, Na^+, rare earth ions, or their mixture, and B contains small highly charged cations like Nb^{5+}, Ta^{5+}, Ti^{4+}, Mo^{6+}, W^{6+}, or V^{5+}. n is the number of octahedral layers in the perovskite layers, and its values vary from 1 to 6.[11−13]

The polarization behavior of BLSFs differs from that of the typical perovskites (e.g., $BaTiO_3$ and $Bi_{0.5}Na_{0.5}TiO_3$) with spontaneous polarization originating from the motion of the B-site ions with respect to their surrounding oxygen octahedral framework. For BLSFs, atomic displacements along the a axis from the corresponding positions in the parent structure (tetragonal, $I4/mmm$) cause ferroelectric spontaneous polarization (P_s).[14] As a consequence of the large coercive field (E_c) and the structural anisotropy of Aurivillius polycrystallines, the piezoelectric coefficient (d_{33}) of most BLSFs with high T_c (T_c > 650 °C) is relatively low, with values ≤20 pC/N found for pure or modified $Bi_4Ti_3O_{12}$ (BIT), $CaBi_4Ti_4O_{15}$ (CBT), $CaBi_2Nb_2O_9$ (CBN), Bi_3TiNbO_9 (BTN), etc.[4,5,15−21] Though $Bi_4Ti_3O_{12}$ (BIT) single crystals have revealed a spontaneous polarization (P_s) of 45−50 $\mu C/cm^2$ along a axis, the obtained P_r of the BIT was only 7.5 $\mu C/cm^2$,[22,23] because of large leakage current and domain pinning due to the presence of defects (mainly oxygen vacancies). Correspondingly, a very low d_{33} (<8 pC/N) is observed for BIT.[24] According to our previous work,[25,26] La substitution for Bi at the A site has been found to be an effective way to increase P_r and d_{33}, through decreasing oxygen vacancy concentration, decreasing leakage current, and increasing poling resistivity. Nevertheless, on account of their close radii [1.36 Å for La^{3+} and 1.38 Å for Bi^{3+}, 12 coordination numbers (CN)],[27,28] the replacement of the asymmetric Bi^{3+} with $6s^2$ lone pair electrons by symmetric La^{3+} could reduce the deformation from the prototype structure, which gives rise to a significant decrease in T_c.[25,26,29] It is adverse to piezoelectric high-temperature applications. So it is expected that the substitution on the A site by other lanthanide cations, with much smaller size than those of Bi^{3+} and La^{3+}, can further improve the ferroelectric properties and piezoelectric properties

Received: December 17, 2012
Published: April 9, 2013

   dx.doi.org/10.1021/ic302769h | Inorg. Chem. 2013, 52, 5045−5054

of BLSFs, without a great decrease in T_c. According to Maiwa et al.,[30] $Bi_{3.25}Nd_{0.75}Ti_3O_{12}$ (BNT) thin films have a larger P_r of 26 $\mu C/cm^2$ and a higher d_{33} of 38 pC/N, as compared to those of La substituted $Bi_{3.25}La_{0.75}Ti_3O_{12}$ (BLT; P_r = 12 $\mu C/cm^2$, d_{33} = 19 pC/N). This could be ascribed to the smaller size of Nd^{3+} (1.27 Å, 12 CN), as compared to that of La^{3+}.[27] Nd substituted Bi_3TiNbO_9 (BTN) polycrystallines also exhibit a remarkable improvement in ferroelectric properties and piezoelectric properties as compared to the pure BTN, and the T_c of them has no significant decrease.[31]

$Na_{0.5}Bi_{2.5}Nb_2O_9$ (NBN) with mixed A-site cations is an important Aurivillius ferroelectric with a high T_c of 790 °C.[32] Additionally, (Li, Ce) and $LiNbO_3$ modified NBN ferroelectrics show excellent piezoelectric properties and high temperature stability.[33,34] In the present work, the $Na_{0.5}Nd_xBi_{2.5-x}Nb_2O_9$ (x = 0.1, 0.2, 0.3, and 0.5; NDBNx, abbreviated as NDBN0.1, NDBN0.2, NDBN0.3, and NDBN0.5, respectively) polycrystallines were prepared by using a solid-state reaction process, and their structures, phase transition behaviors, and electrical properties were studied systematically with the aim of clarifying the effect of Nd substitution.

2. EXPERIMENTAL SECTION

Single phase NDBNx polycrystallines were prepared through solid-state reaction process. Stoichiometric quantities of Bi_2O_3 (99.5%), Nb_2O_5 (99.5%), Na_2CO_3 (99.8%), and Nd_2O_3 (99.99%) were mixed by a ball milling method in ethanol for 24 h. The mixtures were dried and then calcined at 900 °C for 6 h. The calcined powders were remilled in ethanol for 24 h, dried, ground, and cold isostatically pressed into pellets at 400 MPa. The pressed pellets were then sintered at 1100 °C for 2 h, embedded in precursor powders.

Powder X-ray diffraction (XRD) data were collected by using an automated diffractometer (X'Pert PRO MPD, Philips, Eindhoven, The Netherlands) with a nickel filter (Cu Kα radiation) at room temperature. Raman spectra were obtained with an instrument (LabRAM HR800, Horiba Jobin Yvon, Lyon, France) in a backward scattering geometry (the exciting source was the 514.5 nm line from an argon ion laser). Variable-temperature Raman spectra of the samples were stabilized at the desired temperature for 5 min prior to the spectrum measurement. X-ray photoelectron spectroscopy (XPS) measurements were performed with a spectrometer (VG ESCALA-B220i-XL, Thermo Scientific, Surrey, U. K.) with Al Kα (E = 1486.6 eV) radiation. Dielectric properties of the samples were measured by using an LCR meter (4284A, Agilent, CA, U. S. A.). Ferroelectric properties and electrostriction properties were measured by using a ferroelectric analyzer (TF-2000, Aix ACCT, Aachen, Germany). The piezoelectric coefficient (d_{33}) was determined by using a piezo-d_{33} meter (ZJ-3B, Institute of Acoustics, Chinese Academic of Science, Beijing, China). The planar and thickness coupling factors k_p and k_t were determined using the resonance−antiresonance method with a precision impedance analyzer (4294A, Agilent, CA, U. S. A.). Impedance spectroscopy (IS) was performed using an Impedance Analyzer (Solartron, SI 1260, Hampshire, U.K.) in the 0.1 Hz to 10 MHz frequency range at various temperatures.

3. RESULTS AND DISCUSSION

3.1. Structural Refinements and Raman Spectroscopy.

In order to characterize structures of the prepared polycrystallines, XRD Rietveld refinements for the NDBN0.2 and NDBN0.5 were carried out with $A2_1am$ space group at room temperature, by using the GSAS-EXPGUI program.[35,36] The XRD data were collected in a 2θ range of 10−130° with a step size of 0.02° and a step time of 8 s. The coordinates of $Na_{0.5}Bi_{2.5}Nb_2O_9$[37] were used as an initial model where Nd (20%) and Nd (50%) occupied the Bi (4a) site of NDBN0.2 and NDBN0.5, respectively. Acoording to Smolenski et al. and Blake et al.,[38,39] a cation disordering between the A site and the $(Bi_2O_2)^{2+}$ layer, i.e., A-site cation (Na^+ and Nd^{3+}) on the Bi^{3+} site of the $(Bi_2O_2)^{2+}$ layer and Bi^{3+} on the A site, should be considered in the refinement process. The final refined profiles for NDBN0.2 and NDBN0.5 are shown in Figure 1a and b,

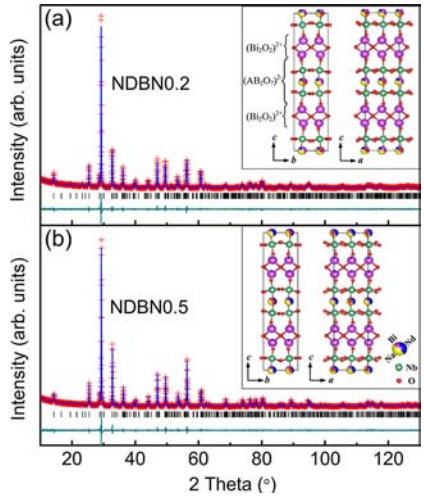

Figure 1. Rietveld refinements for (a) NDBN0.2 and (b) NDBN0.5 at room temperature. The insets show refined crystal structures for them viewed along [100] and [010] directions.

respectively. The final factors, R_{wp}, R_p, and chi-squared values (χ^2) are 10.44%, 7.95%, and 1.472 for NDBN0.2 and 10.39%, 7.85%, and 1.479 for NDBN0.5, respectively, which are listed in Table 1. The refined lattice parameters are a = 5.48558(8) Å, b = 5.46326(9) Å, and c = 24.8940(4) Å for NDBN0.2 and a = 5.46872(5) Å, b = 5.46730(5) Å, and c = 24.80723(25) Å for NDBN0.5. Tables 2 and 3 list the atomic coordinates, atomic occupancies, and isotropic thermal parameters of NDBN0.2 and NDBN0.5, respectively. Selected bond lengths (Å), bond angles (deg), and bond valence calculations (S_{ij})[40] for NDBN0.2 and NDBN0.5 are listed in Table 4. For Nb−O bond lengths in the NbO_6 octahedron, these bond lengths for NDBN0.2 range from 1.833(31) Å to 2.127(30) Å, and those lie between 1.770(14) Å and 2.130(7) Å in NDBN0.5. The bond valence of Bi, Na, and Nd ions in NDBN0.5, both in the

Table 1. Crystal Data and Structure Refinement Conditions for the NDBN0.2 and NDBN0.5

compound	$Na_{0.5}Nd_{0.2}Bi_{2.3}Nb_2O_9$	$Na_{0.5}Nd_{0.5}Bi_2Nb_2O_9$
cryst syst	orthorhombic	orthorhombic
a (Å)	5.48558(8)	5.46872(5)
b (Å)	5.46326(9)	5.46730(5)
c (Å)	24.8940(4)	24.80723(25)
V (Å^3)	746.053(19)	741.715(12)
temperature (K)	298	298
space group	$A2_1am$	$A2_1am$
no. of formula units per unit cell, Z	4	4
no. of reflections	735	733
no. of data points	6000	6000
reduced χ^2	1.472	1.479
R_{int} (%)	4.49	5.01
R_{wp} (%)	10.44	10.39
R_p (%)	7.95	7.85

dx.doi.org/10.1021/ic302769h | Inorg. Chem. 2013, 52, 5045−5054

Table 2. Atomic Coordinates, Atomic Occupancies, and Isotropic Thermal Parameters of the NDBN0.2 at Room Temperature

atom	site	x	y	z	$100U_{iso}$	occupancy
Bi1	4a	0	0.2388(9)	0	0.38(6)	0.356(7)
Na1	4a	0	0.2388(9)	0	0.38(6)	0.4882(24)
Nd1	4a	0	0.2388(9)	0	0.38(6)	0.156(7)
Bi2	8b	0.5071(6)	0.72998(28)	0.19955(5)	1.403(19)	0.972(4)
Na2	8b	0.5071(6)	0.72998(28)	0.19955(5)	1.403(19)	0.0059(12)
Nd2	8b	0.5071(6)	0.72998(28)	0.19955(5)	1.403(19)	0.0220(35)
Nb1	8b	0.4709(6)	0.7462(8)	0.41548(7)	0.02(4)	1
O1	4a	0.450(6)	0.195(6)	0	1.79(27)	1
O2	8b	0.460(4)	0.784(4)	0.3398(6)	1.79(27)	1
O3	8b	0.765(9)	0.008(13)	0.2516(13)	1.79(27)	1
O4	8b	0.656(4)	0.950(4)	0.0855(8)	1.79(27)	1
O5	8b	0.717(6)	0.966(5)	0.5716(7)	1.79(27)	1

Table 3. Atomic Coordinates, Atomic Occupancies, and Isotropic Thermal Parameters of the NDBN0.5 at Room Temperature

atom	site	x	y	z	$100U_{iso}$	occupancy
Bi1	4a	0	0.2430(12)	0	0.14(6)	0.152(7)
Na1	4a	0	0.2430(12)	0	0.14(6)	0.4602(23)
Nd1	4a	0	0.2430(12)	0	0.14(6)	0.388(7)
Bi2	8b	0.4777(10)	0.7372(4)	0.19956(4)	1.818(20)	0.9240(35)
Na2	8b	0.4777(10)	0.7372(4)	0.19956(4)	1.818(20)	0.0199(12)
Nd2	8b	0.4777(10)	0.7372(4)	0.19956(4)	1.818(20)	0.0561(33)
Nb1	8b	0.4784(15)	0.7466(10)	0.41547(6)	0.14(4)	1
O1	4a	0.535(7)	0.208(7)	0	1.65(25)	1
O2	8b	0.442(6)	0.778(6)	0.3449(5)	1.65(25)	1
O3	8b	0.719(10)	0.011(12)	0.2485(16)	1.65(25)	1
O4	8b	0.668(5)	0.942(6)	0.0889(7)	1.65(25)	1
O5	8b	0.759(7)	0.986(9)	0.5700(7)	1.65(25)	1

Table 4. Selected Bond Lengths (Å), Bond Angles (deg), and Bond Valence (S_{ij}) for NDBN0.2 and NDBN0.5

	bond lengths (Å) or angles (deg)		bond valence (S_{ij})	
bond type	NDBN0.2	NDBN0.5	NDBN0.2	NDBN0.5
Bi1/Na1/Nd1−O				
A1−O1	3.025(32) × 1	2.55(4) × 1		
	2.482(32) × 1	2.93(4) × 1		
	2.384(33) × 1	2.47(4) × 1		
	3.106(33) × 1	3.01(4) × 1		
A1−O4	3.253(22) × 2	3.297(26) × 2		
	2.515(21) × 2	2.595(22) × 2	Bi1, 2.509	Bi1, 2.415
A1−O5	2.672(26) × 2	2.555(33) × 2	Na1, 1.142	Na1, 1.100
	2.682(25) × 2	2.686(35) × 2	Nd1, 2.584	Nd1, 2.488
Bi2/Na2/Nd2−O				
Bi2/A2−O2	2.671(22) × 1	2.772(29) × 1		
	2.638(23) × 1	2.747(29) × 1		
Bi2/A2−O3	2.45(5) × 1	2.34(6) × 1		
	2.34(5) × 1	2.32(6) × 1	Bi2, 2.741	Bi2, 2.601
	2.22(5) × 1	2.35(5) × 1	Na2, 1.248	Na2, 1.184
	2.23(5) × 1	2.22(5) × 1	Nd2, 2.823	Nd2, 2.679
Nb−O				
Nb−O1	2.126(5) × 1	2.130(7) × 1		
Nb−O2	1.897(15) × 1	1.770(14) × 1		
Nb−O4	2.034(24) × 1	1.989(31) × 1		
Nb−O4	1.909(24) × 1	1.965(31) × 1		
Nb−O5	2.127(30) × 1	1.92(4) × 1		
Nb−O5	1.833(31) × 1	2.05(4) × 1	Nb, 5.113	Nb, 5.354
Nb−O1−Nb	163.6(17)	159.7(20)		

perovskite layers and in the $(Bi_2O_2)^{2+}$ layers, are lower than those in NDBN0.2. On the contrary, the bond valence of the Nb ion increases as the content of x increases in NDBNx, and its value is +5.113 for NDBN0.2 and +5.354 for NDBN0.5. On the basis of the refined results, the crystal structures of the NDBN0.2 and NDBN0.5 viewed along [100] and [010]

dx.doi.org/10.1021/ic302769h | Inorg. Chem. 2013, 52, 5045−5054

directions at room temperature are depicted in the insets of Figure 1a and b, respectively, with the VESTA program.[41]

Figure 2 shows the evolution of the lattice parameters as the x value increases in NDBNx. With increasing x value, the lattice

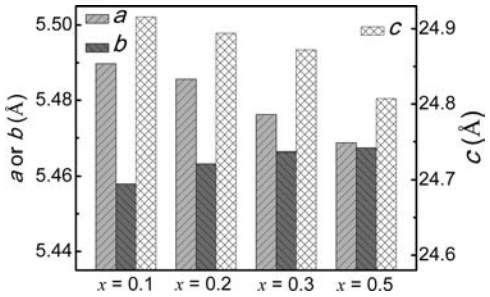

Figure 2. Lattice parameters a, b, and c of the NDBNx.

parameters a and c decrease significantly, while the lattice parameter b increases smoothly. In Aurivillius ferroelectrics, the structural distortion can be mainly described as the tilt of the NbO_6 octahedron about the a axis and the rotation of the NbO_6 octahedron along the c axis, where the neighboring octahedrons rotate in opposite directions.[29] The smaller size Nd^{3+} (1.27 Å, 12 CN) substitution for larger size Bi^{3+} (1.38 Å, 12 CN) seems to induce an enhancement in octahedral tilt about the a axis, which causes a decrease in c. According to Table 4, this angle value of NDBN0.2 and NDBN0.5 is 8.2° [Nb−O1−Nb bond angle: 163.6(17)°] and 10.15° [Nb−O1−Nb bond angle: 159.7(20)°], respectively. However, a reduction of the rotation of the NbO_6 octahedron along the c axis could be brought about owing to the removal of the polarity Bi^{3+} cation with $6s^2$ lone pair electrons at the A site. Correspondingly, the orthorhombicity a/b reduces with increasing Nd concentration.

Raman spectrum of the NDBNx in the range from 30 cm^{-1} to 1250 cm^{-1} are shown in Figure 3a. Raman spectra of the NDBN0.1 exhibit the intense phonon modes at 66, 83, 110, 183, 216, 267, 348, 436, 570, and 819 cm^{-1}, which are related to the orthorhombic phase and are similar to those of SBN.[42−46] The mode at 66 cm^{-1} originates from Bi^{3+} ion vibration in the $(Bi_2O_2)^{2+}$ layers, whereas the modes at 83, 110, and 216 cm^{-1} derive from the vibration of A-site ions in the perovskite layers.[47,48] The mode at 183 cm^{-1} is associated with the vibration of the Nb^{5+} ion along the z direction.[44] By fitting the measured spectra and segregating them into individual Lorentz components, the insets of Figure 3a exhibit the fitting peaks for these modes for all samples. With increasing Nd substitution, the modes at 66 and 216 cm^{-1} demonstrate a visible low-frequency shift, and no obvious frequency shift is observed for the mode at 83 cm^{-1}. Additionally, the mode at 110 cm^{-1} gradually becomes weaker and finally disappears in the NDBN0.5 spectrum. It implies that the Nd^{3+} substitution changes both the A-site cation vibration and the cationic vibration in the $(Bi_2O_2)^{2+}$ layers, which suggests that Nd^{3+} occupies not only the perovskite A site but also the $(Bi_2O_2)^{2+}$ layers. This is consistent with the structural refinement results. The obvious low-frequency shifting for the mode at 183 cm^{-1} may be associated with a significant decrease in lattice parameter c. Additionally, the modes at 267 and 348 cm^{-1} associated with the distortion of the NbO_6 octahedron become weaker with increasing Nd concentration.[49] It suggests that Nd substitution could induce a reduction in orthorhombicity

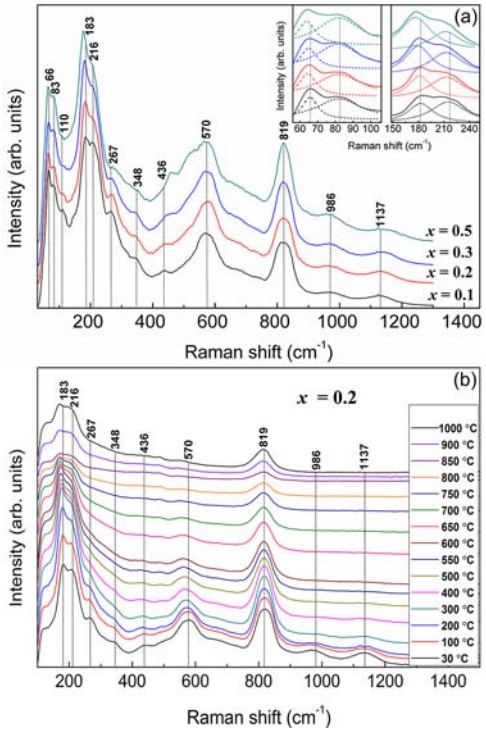

Figure 3. (a) Raman spectra of the NDBNx at room temperature. The insets show regionally enlarged drawings (the solid lines are experimental spectra, and the dotted lines are fitting peaks). (b) Variable-temperature (30−1000 °C) Raman spectra for the NDBN0.2.

distortion. The mode at 436 cm^{-1} exhibits a remarkable high-frequency shift, which is completely dominated by the Bi−O3 force constant.[50] Since the modes at 570 and 819 cm^{-1} are related to the stretching of the O−Nb octahedral chain between two $(Bi_2O_2)^{2+}$ layers,[47,48] no frequency shift for them implies that the B-site Nb^{5+} is not involved in Nd^{3+} substitution. In addition, the spectra of NDBNx reveal two additional modes at 986 and 1137 cm^{-1}, as compared to those of SBN. The two modes could be associated with the lattice distortion and internal force, like the modes at 267 and 348 cm^{-1}.

In order to understand phase transition behavior of the NDBNx, variable-temperature Raman spectra (30−1000 °C) in the range from 100 cm^{-1} to 1300 cm^{-1} for the NDBN0.2 are shown in Figure 3b. It is observed that the modes at 183 and 216 cm^{-1} both exhibit a remarkable low frequency shift with increasing temperature. The mode at 570 cm^{-1} also exhibits a low frequency shift and becomes weaker. This mode corresponds to an unbending sublattice mode and indicates that the equivalent and opposite displacements of positive and negative ions are slightly changed.[42] Additionally, the modes at 267, 348, 436, 986, and 1137 cm^{-1} gradually weaken with increasing temperature. The variation of the above modes against temperature suggests a decrease in atomic displacements from the corresponding positions in the prototype parent structure (tetragonal, $I4/mmm$) and a reduction in distortion of the perovskite layers. Interestingly, the stretching mode of the NbO_6 octahedron at 819 cm^{-1} is not affected by temperature, even up to 1000 °C. It indicates that the motion of the B-site Nb^{5+} with respect to its surrounding oxygen octahedral framework should be not responsible for the ferroelectric to paraelectric phase transition, which is not

dx.doi.org/10.1021/ic302769h | Inorg. Chem. 2013, 52, 5045−5054

identical to that of the typical perovskites (*e.g.*, KNN and PZT). According to Kroumova et al.,[51] the potential modes for the parent phase and the ferroelectric phase $SrBi_2Ta_2O_9$ structure is calculated to be 12 and 84, respectively. Therefore, the characteristic of the low-frequency shifting, the weakening, and the disappearing against temperature could suggest a change in symmetry, from $A2_1am$ to $I4/mmm$. Furthermore, the intensity of the spectra at 750−850 °C is lower than that of other temperature spectra, which indicates that the ferroelectric to paraelectric phase transition of NDBN0.2 may be in this temperature range. From a variable-temperature study, the ferroelectric polarization of NDBN0.2 could be attributed to the distortion of the oxygen octahedron and the ionic displacements deviated from the parent structure.

3.2. Phase Transition Behaviors. The temperature dependence of the real part (ε') and imaginary part (ε'') of dielectric permittivity for the NDBN*x* is shown in Figure 4.

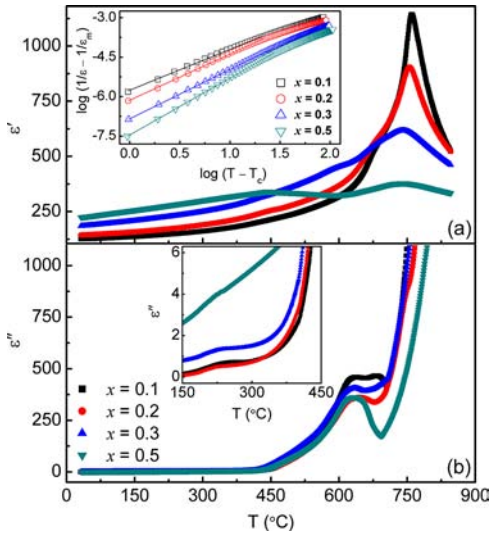

Figure 4. Temperature dependence of the real part (ε') and imaginary part (ε'') of dielectric permittivity for the NDBN*x* at 100 kHz (30−850 °C). (a) ε', with an inset showing the plots of $\log(1/\varepsilon - 1/\varepsilon_m)$ vs $\log(T - T_c)$ for all samples (the symbols, experimental data; the solid lines, fitting to modified CW law). (b) ε'', with an inset showing a regionally enlarged drawing.

According to Figure 4a, the T_c of NDBN*x* ranges from 735 to 764 °C and decreases slightly with increasing Nd concentration. Since the polarity Bi^{3+} cation with $6s^2$ lone pair electrons at the A site causes the deformation from the prototype structure,[29] the substitution of the nonpolarity Nd^{3+} cation should logically decrease orthorhombicity and is supposed to induce a great decrease in T_c for NDBN*x*. On the other hand, this substitution with a much smaller size Nd^{3+} could result in an enhancement in octahedral tilt, which induces an increase in T_c. The offset of these two effects causes a little decrease in T_c of NDBN*x* with introducing Nd. In Figure 4b, an obvious peak is observed in ε'' vs T plots of all samples and locates at about 630 °C. This peak may be associated with the movements of domain walls. Additionally, a small peak associated with point defect dipoles is around 250 °C and becomes much weaker with increasing Nd concentration (inset of Figure 4b). In NDBN*x* polycrystallines, this type of point defect dipole mainly originates from the coupling between an oxygen vacancy ($V_O^{\bullet\bullet}$) and an A-site cation vacancy (V_{Bi}''' or V_{Na}') due to the volatilization of bismuth and sodium. Therefore, one probability is that the Nd substitution contributes to suppressing the defect dipoles through lowering the A-site cation vacancy and oxygen vacancy concentration, which is discussed in the following.

Furthermore, the dielectric peaks become lower and broader with Nd^{3+} substitution. Relaxor ferroelectrics are always characterized by a broadened dielectric peak and strong frequency dispersion. Lead-based PMN, PZN, and Aurivillius phase $BaBi_2Me_2O_9$ (Me = Nd and Ta) demonstrate strong dielectric relaxation behavior. The diffuseness of a phase transition could be described by a modified Curie−Weiss law[52]

$$1/\varepsilon - 1/\varepsilon_m = (T - T_c)^\gamma / C \quad (1)$$

where ε_m is the dielectric permittivity at T_c and C is Curie-type constant. In eq 1, γ ($1 \le \gamma \le 2$) is defined as the diffuseness exponent, which is indicative of the degree of disordering in the ferroelectric−paraelectric transition. By fitting experimental data using eq 1, the γ value of NDBN*x* varies from 1.55 to 2.16 and increases as Nd concentration increases (inset of Figure 4a). Clearly, Nd substitution leads to an increase in degree of relaxation behavior. For Aurivillius relaxors, a cation disordering between the A site and the $(Bi_2O_2)^{2+}$ layer causes their relaxation behaviors. According to the refinement results, small amounts of Na (0.6%) and Nd (2.2%) occupy the Bi (8b) site in the $(Bi_2O_2)^{2+}$ layers in NDBN0.2. Relatively, more Na and Nd occupy the $(Bi_2O_2)^{2+}$ layers in NDBN0.5, and their occupancies are 2.0% and 5.6%, respectively. Clearly, the total content for an A-site cation entering into the $(Bi_2O_2)^{2+}$ layers is about 7.6% in NDBN0.5, much higher than that in NDBN0.2 (about 2.8%). It is suggested that the cation disordering between the A site and the $(Bi_2O_2)^{2+}$ layer is enhanced by increasing Nd substitution and thus very intensive phase transition diffuseness.

3.3. Piezoelectric Properties. After poling in silicone oil in a 100−130 kV/cm dc field at 160 °C for 30−60 min, the d_{33} of all samples was measured at room temperature, which is listed in Table 5. The d_{33} of the NDBN*x* first increases and then decreases as Nd substitution increases. Compared to the pure $Na_{0.5}Bi_{2.5}Nb_2O_9$ (NBN) (d_{33} = 16 pC/N),[26] the NDBN0.2 and NDBN0.3 have a higher d_{33} of 28 pC/N and 27 pC/N, respectively, much higher than the reported d_{33} of other most Aurivillius piezoelectrics with high T_c (T_c > 650 °C, $d_{33} \le 20$ pC/N). The NDBN0.5 has the minimum d_{33}, only 11 pC/N. Commonly, the enhancement of piezoelectric performance is attributed to the increase in spontaneous and remnant polarization. The variation in d_{33} for NDBN*x* seems to be

Table 5. A Comparison of the Properties for the NDBN*x*

compound	T_c (°C)	γ	P_r (μC/cm^2)	E_c (kV/cm)	d_{33} (pC/N)	S_{33} (%)	d_{33}* (pC/N)	k_p (%)	k_t (%)
NDBN0.1	764	1.55	7.2	62.8	25			8.07	14.11
NDBN0.2	755	1.76	9.4	65.5	28	0.04	28.7	8.84	15.47
NDBN0.3	747	1.88	8.2	68.3	27	0.034	25.7	8.69	15.18
NDBN0.5	735	2.16	3.3		11			5.51	9.62

dx.doi.org/10.1021/ic302769h | *Inorg. Chem.* 2013, 52, 5045−5054

compatible with that in P_r, and the higher piezoelectric activity of NDBN0.2 and NDBN0.3 should be closely related to their excellent ferroelectric properties [Table 5 and Figure S2 (Supporting Information)].

Figure 5a shows bipolar field-induced strain for NDBN0.2 and NDBN0.3 measured at 160 °C and 10 Hz. Butterfly-typed

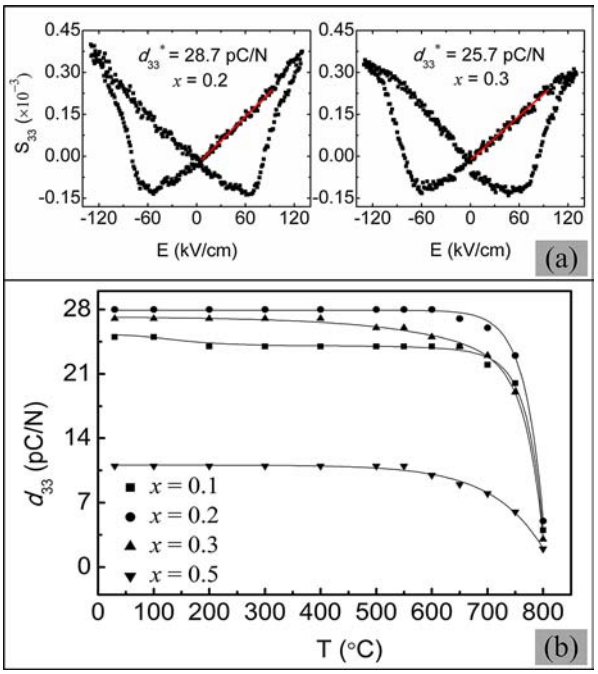

Figure 5. (a) Bipolar electric-field-induced strain for the NDBN0.2 and NDBN0.3 measured at 160 °C and 10 Hz. (b) Effect of annealing temperature (30−800 °C) on piezoelectric activity (d_{33}) of the NDBN*x*.

strain curves are observed, and the strain values (S_{33}) of the NDBN0.2 and NDBN0.3 at 130 kV/cm reach 0.04% and 0.034%, respectively. Aurivillius materials often have lower S_{33} than other ferroelectrics (e.g., PZN-PZT and $Bi_{0.5}Na_{0.5}TiO_3$), because of the two-dimensional orientation restriction of rotation of their spontaneous polarization. Additionally, the piezoelectric constants (d_{33}*) of the NDBN 0.2 and NDBN0.3 are 28.7 and 25.7 pC/N, respectively, calculated directly from the slope of the strain versus electric field curves.[53] For NDBN0.2 and NDBN0.3, these piezoelectric activities are consistent with those measured after dc field poling. Figure 5b shows the effect of thermal depoling on piezoelectric activities of all samples. The d_{33} values were measured at room temperature after annealing for 2 h at each temperature (corresponding to the *x*-axis temperature). Meaningfully, the d_{33} of the NDBN0.2 shows no drop at 600 °C. Even though the annealing temperature is up to 700 °C, the NDBN0.2 still has a higher d_{33} of 26 pC/N. This reveals that the piezoelectric properties of NDBN0.2 are very stable against temperature. For all samples, the d_{33} decreases rapidly when the annealing temperature is near T_c and tends to zero when the temperature is increased above T_c.

3.4. Effect of the Nd Substitution. The isovalent substitution of Nd for Bi has a great influence on structures and properties of the NDBN*x*, e.g., microstructure (grain size and shape), defect concentration (mainly oxygen vacancies), preferred grain orientation (texture) and distortion of the octahedron, and ferroelectric and piezoelectric properties.

First, the Nd substitution reduces the A-site cation vacancies and decreases the concentration of oxygen vacancies, especially around the NbO_6 octahedron. Since A-site cations (Bi^{3+} and Na^+) volatilized during sintering, cation vacancies possibly exist at A sites, which results in oxygen vacancies due to charge neutrality restriction. Compared to that of Na^+, the volatilization of Bi^{3+} brings about more oxygen vacancies because of its higher valence state (+3). When nonvolatile Nd substitutes A-site Bi, the A-site cation vacancy concentration decreases, and the oxygen vacancy concentration of the perovskite layers decreases correspondingly. This can be confirmed by X-ray photoelectron spectroscopy (XPS). Figure 6 shows Bi 4f XPS spectra of the nonsputtered and 1 min

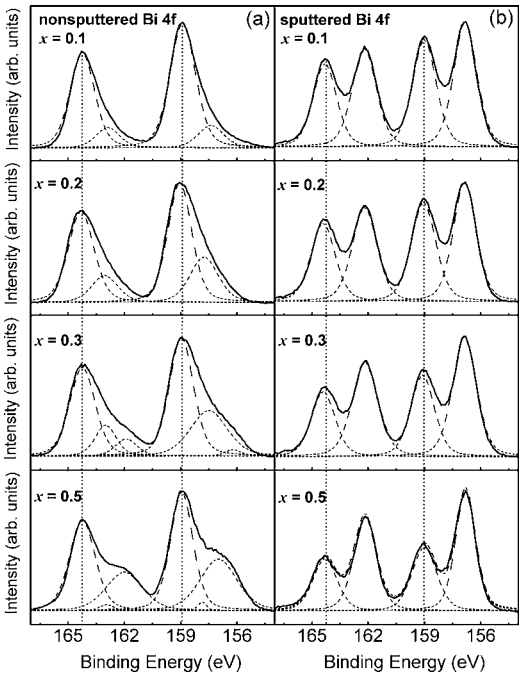

Figure 6. (a) Nonsputtered and (b) sputtered Bi 4f XPS spectra for NDBN*x* samples (the solid lines are experimental spectra, and the dotted lines are fitting peaks).

sputtered NDBN*x* samples. For the nonsputtered (Figure 6a), the major 7/2 and 5/2 spin−orbit doublet components of the Bi 4f spectra are located at 158.9 and 164.3 eV, respectively. With Gauss−Lorentz method fitting, one or two additional small doublet peaks are observed at low binding energy sides, and their relative intensity increases as Nd concentration increases. After sputtering (Figure 6b), those doublet peaks with low energy in NDBN*x* spectra become more intensive and locate at about 156.8 and 162.2 eV, respectively, which may come from a suboxidated bismuth state with Bi^{+3-x}, while the major Bi 4f doublet peaks at high energy besides remain unchanged, which are assigned to the oxidized bismuth (Bi^{3+}). Interestingly, the relative intensity of the Bi^{+3-x} peak increases with increasing Nd amount, as compared to that of the Bi^{3+} components, which is consistent with that of La substituted $Bi_4Ti_3O_{12}$.[54] Determined by the occupancy and the bismuth valence state for Bi1 at the A site and Bi2 in the $(Bi_2O_2)^{2+}$ layers (Tables 2−4), the total Bi valence for NDBN0.2 and NDBN0.5 is calculated to be +2.705 and +2.587, respectively. It indicates that the existence of the underbonded Bi cation is more pronounced in NDBN0.5, which leads to an increase in

dx.doi.org/10.1021/ic302769h | Inorg. Chem. 2013, 52, 5045−5054

relative intensity of its suboxidated peak. According to Figure 7a and b, for all samples, the peak position and shape of Nd 3d

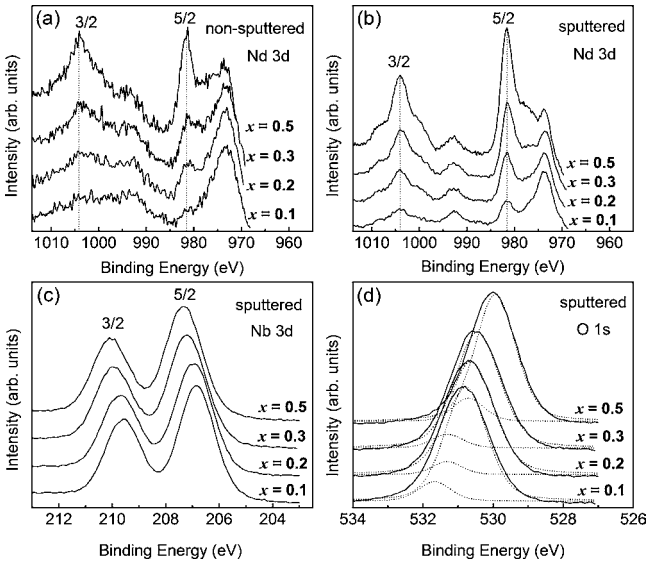

Figure 7. (a) Nonsputtered and (b) sputtered Nd 3d XPS spectra for NDBN*x* samples. (c) Sputtered Nb 3d XPS spectra for NDBN*x* samples. (d) Sputtered O 1s XPS spectra for NDBN*x* samples (the solid lines are experimental spectra and the dotted lines are fitting peaks).

spectra are not affected by sputtering, except for the increase of peak intensity. When comparing Bi 4f to Nd 3d spectra, it is indicated that the oxygen ions near Nd ions are more stable than those near Bi ions, and the oxygen vacancies are more likely present in the vicinity of Bi ions.

Furthermore, it is observed that the sputtered Nb 3d spectra shift to higher binding energies with increasing Nd concentration (Figure 7c). It suggests that Nd substitution causes a decrease in oxygen vacancy concentration around the NbO_6 octahedron. Figure 7d shows the sputtered O 1s spectra of the NDBN*x*. With Gauss−Lorentz method fitting, two different component peaks are obtained, and the first peak at the low binding energy side corresponds to the Nb−O bond, and the second peak is ascribed to the oxygen attached to the A-site cation.[55] Clearly, the two peaks both shift into lower energies as the Nd concentration increases. This suggests that the electronegativity of oxygen ions becomes higher with increasing Nd substitution, from both A−O and Nb−O bonds. Overall, the Nd substitution for A-site Bi causes the number of oxygen vacancies to decrease massively, especially in the perovskite layers. For BLSFs, the conductivity behavior and ferroelectric polarization mainly originate from the perovskite layers, and the $(Bi_2O_2)^{2+}$ layers are the rigid insulative and nonpolarity slabs. So the reduction of oxygen vacancies in the perovskite layers contributes to the decrease of leakage current and the suppression of domain-wall pinning, and thus higher d_{33}.

Second, a decrease in oxygen vacancy concentration could result in slow transport of oxygen ions, hence inhibiting the grain growth.[56] The inhibition of grain growth may produce two contrary effects. (I) The first is a decrease in tendency to growing in the *ab* plane. This would lower the aspect ratio L/T (length/thickness of grain) and decrease the probability of the grain *c*-orientation (Supporting Information, Figure S1). For two-layer Aurivillius oxides, the ferroelectric polarization (P_s) mainly originates from the *ab* plane, and the higher *c*-orientation is adverse to large P_r and high d_{33}. As a result, there may be more crystallographic directions suitable for polarization, facilitating piezoelectricity. Additionally, owing to a different ratio for L/T (length/thickness of grain) accompanying a decrease in L/T, polycrystallines tend to become more dense after sintering, and a sound grain growth could be obtained, e.g., NDBN0.2 and NDBN0.3 samples (Supporting Information, Figure S1 and Table S1). The enhancements of piezoelectric properties of the NDBN0.2

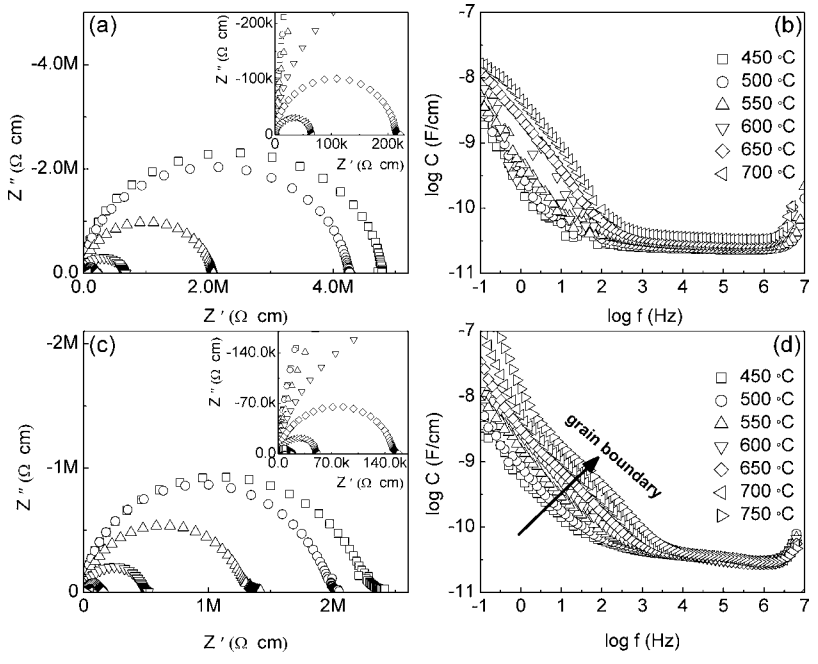

Figure 8. *Z** plots and *C*′ spectroscopic plots over 450−750 °C for the NDBN0.2 and NDBN0.5 with a Ag electrode. (a) *Z** for NDBN0.2. (b) *C*′ for NDBN0.2. (c) *Z** for NDBN0.5. (d) *C*′ for NDBN0.5.

dx.doi.org/10.1021/ic302769h | *Inorg. Chem.* 2013, 52, 5045−5054

and NDBN0.3 were partly contributed from the effect of grain size.[57] (II) The second effect is a smaller grain size, which could induce a higher volume of grain boundaries and an outstanding grain-boundary effect. In order to elucidate the probably outstanding grain-boundary effect caused by Nd substitution, the impedance spectroscopy (IS) approach was invoked, which is a useful technique to characterize electroceramics and is particularly helpful to separate grain, grain boundary, and electrode effects.[58] Figure 8 shows impedance complex plane (Z^*) and C' spectroscopic plots at 450−750 °C for NDBN0.2 and NDBN0.5. Commonly, IS data can be modeled on an equivalent circuit consisting of three parallel RC elements connected in series, electrode, grain boundary, and grain components, respectively, from low frequency to high frequency. However, only a single, essentially undistorted Debye-like semicircle is observed for NDBN0.2 at each temperature (Figure 8a). This indicates that the NDBN0.2 sample contains essentially one electrical component. Comparatively, for NDBN0.5, a second electrical component becomes apparent at the low frequency range (Figure 8c). Correspondingly, the C' spectroscopic plots of NDBN0.2 (Figure 8b) show a low capacitance plateau, about 0.023 nF/cm at the 100−1 M Hz range. But apart from a low capacitance plateau at 10 000 to 1 M Hz, a high capacitance plateau (about 1 nF/cm) is observed at low frequency range for NDBN0.5 (Figure 8d). According to Li et al.,[59] the low capacitance plateau (0.023 nF/cm) is referred to grain effects, whereas the high capacitance plateau (about 1 nF/cm) is ascribed to grain boundary effects. It is suggested that the capacitance of NDBN0.2 is dominated by the classic bulk response. Dissimilarly, two components associated with grain and grain boundary effects attribute to Z^* and C' of NDBN0.5. Logarithmic conductivity (450−750 °C) of NDBNx obtained from the low-frequency intersects of the impedance complex plane data in their Z^* plots are shown in Figure 9. It can be

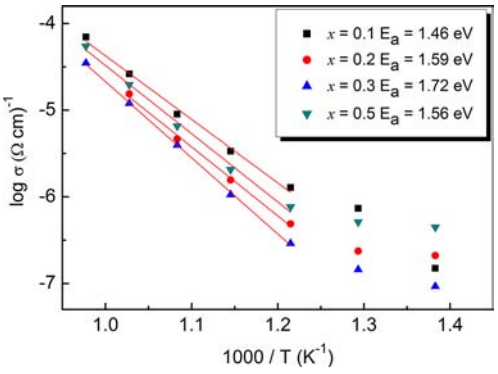

Figure 9. Temperature dependence of logarithmic conductivity for NDBNx over 450−750 °C.

seen that a good linear fitting for log σ vs 1000/T plots of all samples at a higher temperature range (550−750 °C) and the activation energy (E_a) is 1.46−1.72 eV, corresponding to the intrinsic conduction. Interestingly, with increasing Nd concentration, a significant decrease in conductivity is observed in NDBN0.2 and NDBN0.3, while the conductivity of NDBN0.5 increases abnormally. The decrease of grain conductivity of NDBN0.2 and NDBN0.3 should be attributed to the reduction of the defects present in the lattice, especially in the perovskite lattice, which induces an increase in E_a in them. For NDBN0.5, apart from grain conductivity, the outstanding grain-boundary conductivity may contribute to its higher conductivity and lower E_a, because of space charges and defects (such as Na^+, Fe^{3+}, Cl^-, etc., which are abundant in nature[60]) mainly concentrating on grain boundaries. Therefore, the piezoelectric activity of NDBN0.5 could be suppressed by compensated charge and large mechanical stresses resulting from grain boundaries, through preventing domain reversal with external fields and inducing the degradation of ferroelectric performance in terms of polarization, electric leakage current, dielectric strength, etc.[60−62]

Third, the substitution of Nd^{3+} for polarity Bi^{3+} could result in a decrease in spontaneous polarization (P_s). For two-layer Aurivillius oxides with $A2_1am$ orthorhombic symmetry, atomic displacements along the a axis from the corresponding positions in the parent tetragonal ($I4/mmm$) cause ferroelectric spontaneous polarization (P_s). Polarizations originating from the displacements along b and c axes are canceled because of the presence of glide and mirror planes, respectively. On the basis of the atomic displacements, total P_s of the displace-type ferroelectrics is calculated by using Shimakawa's mode[63]

$$P_S = \sum_i \frac{m_i \times \Delta x_i \times Q_i e}{V} \quad (2)$$

where m_i is the site multiplicity, Δx_i is the atomic displacement along the a axis from the corresponding position in the parent structure, $Q_i e$ is the ionic charge for the ith constituent ion, and V is the volume of the unit cell. In terms of the refined crystallographic data (Tables 1−3), the ion displacements along the a axis and the contributions of each constituent ion to the total P_s for NDBN0.2 and NDBN0.5 are shown in Figure 10 (the position of the A site on the a axis is fixed at the origin). Apparently, the calculated P_s of NDBN0.2 (22.9 μC/cm^2) is much larger than that of NDBN0.5 (11.6 μC/cm^2). It implies that the Nd substitution could result in a decline in ferroelectric polarization and a decrease in P_r correspondingly (Supporting Information, Figure S2), in NDBN0.5. This seems to be associated with a relaxation of the structural orthorhombicity due to the symmetric Nd^{3+} substitution for the asymmetric Bi^{3+}. In addition, the observed P_s of the two compounds (about 10.2 and 3.5 μC/cm^2 for NDBN0.2 and NDBN0.5, respectively; Supporting Information, Figure S2) is much lower than the calculated, which should be ascribed to the highly randomly oriented characteristic and large coercive field of Aurivillius phase polycrystallines.

Therefore, it is concluded that the excellent ferroelectric properties and piezoelectric properties of the NDBN0.2 should originate from the reduction of defects (mainly oxygen vacancies in the perovskite layers), the depression of the leakage current, and a sound grain growth. In contrast, the outstanding grain-boundary effects accompanying smaller grain size, higher volume of grain boundaries, and larger internal stresses and a decrease in orthorhombicity polarization may be the answer for the smaller P_r and lower d_{33} of NDBN0.5.

4. CONCLUSIONS

New Aurivillius phase ferroelectrics $Na_{0.5}Nd_xBi_{2.5-x}Nb_2O_9$ (NDBNx, x = 0.1, 0.2, 0.3, and 0.5) with Nd substitution for Bi were synthesized using a solid state reaction process. The refinement results and Raman spectroscopy of NDBNx verified that Nd occupies both the A site in the perovskite and the cation site in the $(Bi_2O_2)^{2+}$ layers. The Nd substitution for Bi resulted in a reduction in A-site vacancies and a significant

dx.doi.org/10.1021/ic302769h | Inorg. Chem. 2013, 52, 5045−5054

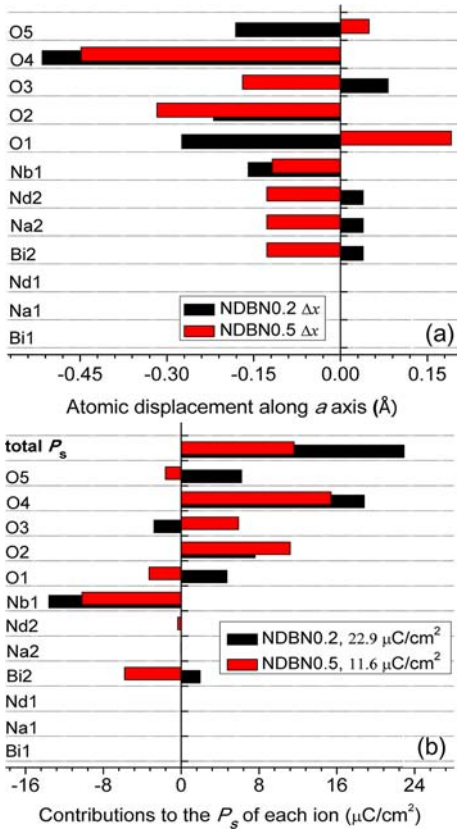

Figure 10. (a) Ion displacement and (b) contribution to the total spontaneous polarization (P_s) of each ion in the NDBN0.2 and NDBN0.5.

decrease in oxygen vacancy concentration (especially in the perovskite layers), a decrease in grain size, an increase in internal strain, and a decrease in orthorhombicity polarization. The coaction between these effects determined the structure characteristics, phase transition behaviors, and electrical properties of NDBN*x*. The ferroelectric to paraelectric phase transition temperature (T_c) of NDBN*x* ranged from 735 to 764 °C. With increasing Nd substitution, the T_c of NDBN*x* decreased slightly, whereas their relaxation behavior originating from the cation disordering between the A site and the $(Bi_2O_2)^{2+}$ layer became more and more intensive. The NDBN0.2 had a larger remnant polarization (P_r) of 9.4 $\mu C/cm^2$, a larger field-induced strain (S_{33}) of 0.04%, and a higher piezoelectric coefficient (d_{33}) of 28 pC/N, with a high T_c of 755 °C. Interestingly, the piezoelectric properties of NDBN0.2 were very stable against temperature. Our results suggest that the piezoelectric NDBN0.2 is a promising candidate for use in high temperature applications.

■ ASSOCIATED CONTENT

Supporting Information

Lattice parameters, cell volume and density of the NDBNx ceramics. Powder XRD and surface SEM images of the NDBNx polycrystallines. *P*–*E* and *I*–*E* loops of the NDBNx measured at 160 °C and 10 Hz. This material is available free of charge via the Internet at http://pubs.acs.org.

■ AUTHOR INFORMATION

Corresponding Author

*Tel.: +86 29 88494463. Fax: +86 29 88492642. E-mail: hqfan3@163.com and longchangbai@126.com.

Notes

The authors declare no competing financial interest.

■ ACKNOWLEDGMENTS

This work was supported by the National Natural Science Foundation (51172187), the SRPDF (20116102130002) and 111 Program (B08040) of MOE, the Xi'an Science and Technology Foundation (CX1261-2, CX1261-3) of China.

■ REFERENCES

(1) Paz de Araujo, C. A.; Cuchiaro, J. D.; McMillan, L. D.; Scott, M. C.; Scott, J. F. *Nature* **1995**, *374* (6323), 627–629.
(2) Park, B. H.; Kang, B. S.; Bu, S. D.; Noh, T. W.; Lee, J.; Jo, W. *Nature* **1999**, *401*, 682–684.
(3) Scott, J. F.; Paz de Araujo, C. A. *Science* **1989**, *246*, 1400–1405.
(4) Yan, H. X.; Zhang, H. T.; Ubic, R.; Reece, M. J.; Liu, J.; Shen, Z.; Zhang, Z. *Adv. Mater.* **2005**, *17*, 1261–1265.
(5) Yan, H. X.; Zhang, H. T.; Reece, M. J.; Dong, X. L. *Appl. Phys. Lett.* **2005**, *87*, 0829111–3.
(6) Whittle, K. R.; Hyatt, N. C.; Reaney, I. M. *Chem. Mater.* **2008**, *20* (20), 6427–6433.
(7) Oh, S. J.; Shin, Y. T.; Thao, T. T.; Lee, D. W.; Yoon, A.; Halasyamani, P. S.; Ok, K. M. *Inorg. Chem.* **2012**, *51* (19), 10402–10407.
(8) Garnweitner, G.; Hentschel, J.; Antonietti, M.; Niederberger, M. *Chem. Mater.* **2005**, *17* (18), 4594–4599.
(9) Fraysse, G.; Rouquette, J.; Haines, J.; Bornand, V.; Papet, P.; Pereira, A. S. *Inorg. Chem.* **2012**, *51* (23), 12619–12625.
(10) Zhou, Z.; Dong, X.; Chen, H. *J. Am. Ceram. Soc.* **2006**, *89*, 1756–1760.
(11) Aurivillius, B. *Ark. Kemi* **1949**, *1*, 463–480.
(12) Aurivillius, B. *Ark. Kemi* **1950**, *2*, 519.
(13) Aurivillius, B. *Ark. Kemi* **1952**, *5*, 39.
(14) Withers, R. L.; Thompson, J. G.; Rae, A. D. *J. Solid State Chem.* **1991**, *94*, 404–417.
(15) Yan, H. X.; Zhang, H. T.; Zhang, Z.; Ubic, R.; Reece, M. J. *J. Eur. Ceram. Soc.* **2006**, *26*, 2785–2792.
(16) Villegas, M.; Jardiel, T.; Farias, G. *J. Eur. Ceram. Soc.* **2004**, *24*, 1025.
(17) Zhang, X. D.; Yan, H. X.; Reece, M. J. *J. Am. Ceram. Soc.* **2008**, *91*, 2928–2932.
(18) Zeng, J. T.; Li, Y. X.; Wang, D.; Yin, Q. R. *Solid State Commun.* **2005**, *133*, 553.
(19) Zhang, X.; Huang, Z.; Chan, H.; Kwok, K.; Choy, C. *J. Eur. Ceram. Soc.* **1999**, *19*, 985.
(20) Yan, H. X.; Zhang, Z.; Zhu, W. M.; He, L. X.; Yu, Y. H.; Li, C. G.; Zhou, J. G. *Mater. Res. Bull.* **2004**, *39*, 1237–1246.
(21) Takenaka, T.; Sakata, K. *J. Appl. Phys.* **1984**, *55*, 1092–9.
(22) Takahashi, M.; Noguchi, Y.; Miyayama, M. *Solid State Ionics* **2004**, *172*, 325–329.
(23) Du, X.; Chen, I. W. *J. Am. Ceram. Soc.* **1998**, *81*, 3253–3259.
(24) Hou, J. G.; Qu, Y. F.; Vaish, R.; Krsmanovic, D.; Varma, K. B. R.; Kumar, R. V. *J. Am. Ceram. Soc.* **2010**, *93*, 1414–1421.
(25) Long, C. B.; Fan, H. Q. *Dalton Trans.* **2012**, *41*, 11046–11054.
(26) Long, C. B.; Fan, H. Q.; Li, M. M.; Li, Q. *CrystEngComm* **2012**, *14*, 7201–7208.
(27) Shannon, R. D. *Acta Crystallogr., Sect. A: Cryst. Phys., Diffr., Theor. Gen. Crystallogr.* **1976**, *A32*, 751–767.
(28) Sivakumar, T.; Itoh, M. *Chem. Mater.* **2011**, *23*, 129–131.
(29) Frit, B.; Mercurio, J. P. *J. Alloys Compd.* **1992**, *188*, 27–35.
(30) Maiwa, H.; Iizawa, N.; Togawa, D.; Hayashi, T.; Sakamoto, W.; Yamada, M.; Hirano, S. *Appl. Phys. Lett.* **2003**, *82* (11), 1760–1762.

(31) Zhang, H. T.; Yan, H. X.; Reece, M. J. *J. Appl. Phys.* **2009**, *106*, 0441061−5.
(32) Aoyagi, R.; Takeda, H.; Okamura, S.; Shiosaki, T. *Mater. Res. Bull.* **2003**, *38*, 25−32.
(33) Gai, Z. G.; Wang, J. F.; Zhao, M. L.; Wang, C. M.; Zang, G. Z.; Ming, B. Q.; Qi, P. S.; Zhang, J.; Shrout, T. R. *Appl. Phys. Lett.* **2006**, *89* (012907), 1−3.
(34) Jiang, X.; Yang, Q.; Zhou, S.; Chen, C.; Chen, Y.; Tu, N.; Yu, Z. *J. Am. Ceram. Soc.* **2011**, *94*, 1109−1113.
(35) Larson, A. C.; Von Dreele, R. B. *General Structure Analysis System (GSAS)*; LANL Report LAUR 86-748, Los Alamos National Laboratory: Los Alamos, NM, 2000.
(36) Toby, B. H. *J. Appl. Crystallogr.* **2001**, *34*, 210−213.
(37) Borg, S.; Svensson, G. *J. Solid State Chem.* **2001**, *156*, 160−165.
(38) Smolenski, G. A.; Isupov, V. A.; Sov, A. *Phys. Solid State (Engl. Transl.)* **1959**, *3*, 651.
(39) Blake, S. M.; Falconer, M. J.; McCreedy, M.; Lightfoot, P. *J. Mater. Chem.* **1997**, *7*, 1609−1613.
(40) Brown, I. D.; Altermatt, D. *Acta Crystallogr., Sect. B* **1985**, *41*, 244−247.
(41) Momma, K.; Izumi, F. *J. Appl. Crystallogr.* **2008**, *41* (3), 653−658.
(42) Fang, P. Y.; Fan, H. Q.; Li, J.; Liang, F. J. *J. Appl. Phys.* **2010**, *107* (064104), 1−4.
(43) Das, R. R.; Perez, W.; Katiyar, R.; Bhalla, A. S. *J. Raman Spectrosc.* **2002**, *33*, 219−222.
(44) Liu, G. Z.; Wang, C.; Gu, H. S.; Lu, H. B. *J. Phys. D: Appl. Phys.* **2007**, *40*, 7817−7820.
(45) Verma, M.; Sreenivas, K.; Guptaa, V. *J. Appl. Phys.* **2009**, *105*, 0245111−0245116.
(46) Volanti, D. P.; Cavalcante, L. S.; Paris, E. C.; Simões, A. Z.; Keyson, D. *Appl. Phys. Lett.* **2007**, *90*, 2619131−3.
(47) Zhou, Z. Y.; Dong, X. L.; Yan, H. Y. *Scr. Mater.* **2006**, *55*, 791−794.
(48) Liang, K.; Qi, Y. J.; Lu, C. J. *J. Raman Spectrosc.* **2009**, *40*, 2088−2091.
(49) Liu, J. J.; Zou, G. T.; Jin, Y. R. *J. Phys. Chem. Solids.* **1996**, *51*, 1653−1658.
(50) Gupta, H. C.; Archana; Luthra, V. *Vib. Spectrosc.* **2011**, *56*, 235−240.
(51) Kroumova, E.; Aroyo, M. I.; Perez Mato, J. M.; Kirov, A.; Capillas, C.; Ivantchev, H.; Wondratschek, H. *Phase Transitions* **2003**, *76*, 155−170.
(52) Uchino, K.; Nomura, S. *Ferroelectr., Lett. Sect.* **1982**, *44*, 55.
(53) Fan, H. Q.; Kim, H. E. *J. Appl. Phys.* **2002**, *91* (1), 317−322.
(54) Chu, M. W.; Ganne, M.; Caldes, M. T.; Brohan, L. *J. Appl. Phys.* **2002**, *91*, 3178−3187.
(55) Jovalekic, C.; Pavlovic, M.; Osmokrovic, P.; Atanasoska, L. *Appl. Phys. Lett.* **1998**, *72* (9), 1051−1053.
(56) Shimanskij, A. F.; Drofenik, M.; Kolar, D. *J. Mater. Sci.* **1994**, *29*, 6301−6305.
(57) Hou, J. G.; Kumar, R. V.; Qu, Y. F.; Krsmanovic, D. *Scr. Mater.* **2009**, *61*, 664−667.
(58) Irvine, J. T. S.; Sinclair, D. C.; West, A. R. *Adv. Mater.* **1990**, *2*, 132.
(59) Li, M.; Sinclair, D. C. *J. Appl. Phys.* **2012**, *111*, 0541061−0541068.
(60) Du, H. C.; Tang, L. J.; Kaskel, S. *J. Phys. Chem. C* **2009**, *113*, 1329−1339.
(61) Lines, M. E.; Glass, A. M. *Principles and Applications of Ferroelectrics and Related Materials*: Oxford University: Oxford, U. K., 1977.
(62) Lee, J. S.; Joo, S. K. *Appl. Phys. Lett.* **2002**, *81*, 2602.
(63) Shimakawa, Y.; Kubo, Y.; Nakagawa, Y.; Goto, S.; Kamiyama, T.; Asano, H.; Izumi, F. *Phys. Rev. B* **2000**, *61*, 6559−6564.